Comparison of LCC Solder Joint Life Predictions With Experimental Data

Liang-chi Wen

Ronald G. Ross, Jr.

Jet Propulsion Laboratory,
California Institute of Technology,
Pasadena, CA 91109

The ability of solder joint life-prediction algorithms to predict the failure of solder joints due to temperature-cycling induced creep-fatigue has been investigated using representative leadless chip carriers (LCCs) as the test vehicle. Four different algorithms are assessed: the classic Coffin-Manson algorithm, a modified Coffin-Manson algorithm with dependency on peak stress, and two strain-energy based algorithms. JPL's special purpose nonlinear finite element computer program was used to dynamically simulate the solder joint response to the standard NASA temperature cycling environment, which ranges from −55°C to +100°C with a 4-hour period. The computed stress-strain history provided the inputs needed by each of the failure algorithms. To test the accuracy of the analytical predictions, three different sizes of LCCs (68 pins, 28 pins, and 20 pins) were subjected to an experimental test program using the same 4-hour temperature cycle as used in the analytical predictions. The three different sized ceramic packages, each with a 50-mil pitch, provided a range of cyclic strain ranges and solder fillet geometries so as to test the algorithms against realistic electronic packaging variables. The study highlights limitations in the historical Coffin-Manson relationship, and points up possible improvements associated with incorporating a stress modifier into the Coffin-Manson equation. This modification is also somewhat simpler and more accurate than the energy-density based algorithms, which also performed quite well.

Introduction

One of the inherent reliability problems for surface mount applications is that solder joints, which perform both electrical and mechanical connections between parts and boards, are subjected to thermal/mechanical fatigue failure. Service life of solder joints depends upon many factors including solder metallurgical composition, the design and material selection of the part/board assembly, and the thermal/mechanical service environment. Solder joint deterioration involves a sequence of local straining, micro-cracking, crack initiations and crack propagation, resulting eventually in total joint separation from the PWB footprint.

Solder joint service life prediction is a crucial part of the overall methodology to ensure solder integrity for surface mount applications. A validated life prediction methodology is an important tool for packaging design, as well as for the development of quality inspection and qualification testing guidelines. Because of this need, reliability prediction methods have been continuously upgraded over the years. Many different approaches have been reported in the literature, ranging from simple empirical formulas to complex multi-node finite-element models.

Unfortunately, the state-of-the-art of assessing solder joint integrity is still far from mature. Because of the inherent weaknesses in the available prediction tools, current design practices must rely heavily on extrapolating historical performance data and using accelerated testing techniques. Improved prediction techniques would lessen the bias against the introduction of new products and applications, and would improve the design process itself by clarifying the critical life-determining issues.

Contributed by the Electrical and Electronic Packaging Division and presented at the International Mechanical Engineering Congress and Exposition, Chicago, IL, November 6–11, 1994 of The American Society of Mechanical Engineers. Manuscript received by the EEPD August 1994; revised manuscript received March 31, 1995. Paper No. 94-WA/EEP-13. Associate Technical Editor: J. H. Lau.

To help assess the strengths and limitations of the current life prediction algorithms, and to identify possible improvements, a combined analytical experimental program has been carried out using a variety of the more popular failure prediction algorithms. The analytical life-prediction results are contrasted with the measured failure trends of three sizes of Leadless Chip Carriers (LCCs) whose lives were measured in a standard NASA −55°C to +100°C thermal-cycle test.

Life Prediction Computational Elements

Before discussing the details of the studied failure prediction algorithms, it is important to note that the failure algorithms themselves are only a portion of the total life prediction computation. The total computation can be thought of as being composed of three elements:

- Modeling the external thermal/mechanical loading environment
- Computing the resulting stress/strain history within the solder joints
- Predicting the damage accrual and failure probability given the computed stress/strain history

Although the principal focus of this paper is on the last element, i.e., exploring the strengths and weaknesses of various damage accrual and failure prediction models, the external environment, physical dimensions, and stress/strain prediction are so closely intertwined that they must at least be briefly discussed to place the subsequent discussion in context.

External Thermal/Mechanical Loading Environment. When discussing the structural failure of an electronic part soldered to a PWB, the fundamental initiator of the failure is the external loading environment. The most common external loading environment is cyclic temperature or deflection loading of the assembly. Cyclic temperature results in cyclic mechanical loads caused by differential thermal expansions of the system due to combinations of both thermal gradients and interlocking

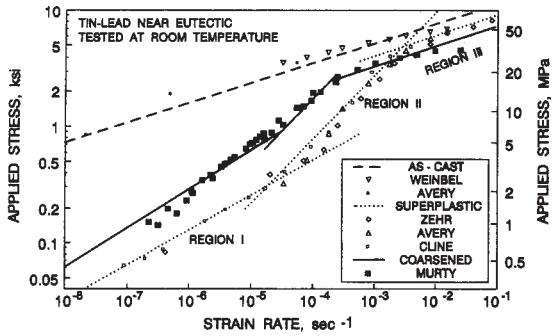

Fig. 1 Dependence of stress/strain-rate constitutive properties of room-temperature eutectic Sn-Pb solder on metallurgical aging condition

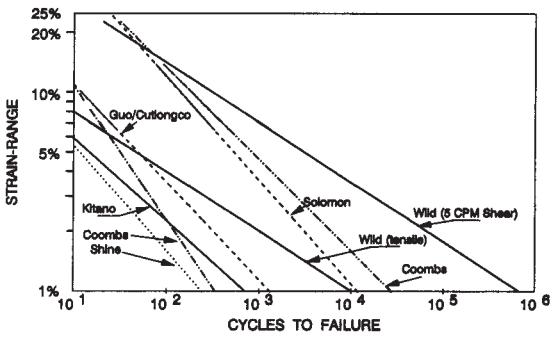

Fig. 3 Coffin-Manson fatigue plots for room-temperature eutectic Sn-Pb solder as reported by various investigators

materials with different coefficients of thermal expansion (CTE). Thermal cycling away from room temperature also requires the consideration of temperature dependent material properties, which are particularly significant for solder and many polymer materials. Because solder also displays important time and rate dependencies, such as creep and strain rate effects, the rate of the applied load and the length of dwell periods are also important parameters that must be carefully included.

Stress/Strain Prediction Models. Given a cyclic temperature or cyclic external loading environment, the damage generated in an individual solder joint is fundamentally driven by the time history of the stresses and strains that are developed in the solder joint. Computing the time history of stresses and strains requires knowledge of the external loading environment, the detailed geometry of the system, and the time and temperature dependent thermal/mechanical properties of the various materials making up the system. Because of the importance of the time and temperature dependence of solder properties, the structural model must accurately address these dependencies by including the complete constitutive properties of the solder as highlighted in Figs. 1 and 2. At JPL, this is done in a special in-house finite element creep-fatigue simulation computer program, which calculates the solder elemental stresses and strains as a function of time (Ross et al., 1992). All stress-strain histories used for the analytical life predictions described in this paper were computed using this specialized JPL program.

Failure Prediction and Damage Accrual Models

The key focus of this paper is on the last element of the life prediction process—that of predicting the level of damage or probability of failure given an accurately computed time history of stress and strain within the solder joint.

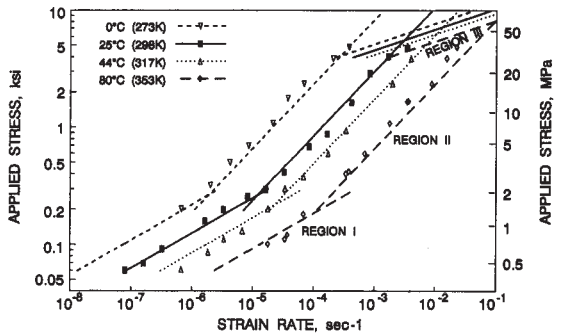

Fig. 2 Dependence of stress/strain-rate constitutive properties of eutectic Sn-Pb solder on operating temperature

A number of failure prediction algorithms have been derived over the years from experimental observations of fatigue behavior together with knowledge of the physics of failure. Although there are numerous variations and modifications, the algorithms can be categorized into four generic groups: (1) stress-range based, (2) strain-range based, (3) strain-energy based, and (4) fracture-mechanics based. Because stress-range and fracture-mechanics based approaches are not commonly used for low cycle fatigue in ductile materials, the discussion in this paper has been limited to the Coffin-Manson and strain-energy based algorithms.

Because the exact definition of failure is important for accurate comparisons, a consistent definition must be used for all algorithms as well as for the experimental measurements. Over the years, many definitions of failure have been used by the solder research community; these include such definitions as 50 percent peak load drop, 10 percent increase in electrical resistance, initiation of a visible crack, and complete fracture of the solder joint. This paper adopts the latter, i.e., a complete fracture of the solder joint, thus causing an electrical open circuit between the part and the PWB. More precisely, end of life is defined here as the time (or number of thermal cycles) when the weakest solder joint on an electronic part has a 50 percent probability of complete open-circuit failure. This definition recognizes that the first failure is the key one, and that once the weakest solder joint has failed, the load is shifted to the remaining joints in a manner that greatly alters the failure distribution of the remaining joints on the part. In analytical modeling this is not particularly important; however, it is critical in comparing analytical results with experimental measurements.

Strain-Range Coffin-Manson Algorithms. Historically, the overwhelming majority of solder fatigue life predictions have been conducted using strain-range based failure criterion. Total strain range, $\Delta\epsilon_t$, is made up of an elastic strain, $\Delta\epsilon_e$, which is negligible in most practical low-cycle fatigue applications, and a non-elastic plastic/creep strain $\Delta\epsilon_p$, which is the primarily damage generator. The strain-range failure algorithm relates the projected fatigue life (number-of-cycles-to-failure) to the cyclic plastic strain range by Eq. (1). This equation, which is commonly referred to as the Coffin-Manson equation, was developed independently by Coffin (1954) and Manson (1953):

$$\Delta\epsilon_p = CN_f^{-k} \tag{1}$$

where

N_f = number of cycles to failure
k = ductility exponent
$\Delta\epsilon_p$ = plastic strain range
C = material coefficient

A major source of confusion in the current art of solder life prediction is the order-of-magnitude variability in the reported values for the constants in Eq. (1). Figure 3 and Table 1 show

Table 1 Coffin-Manson parameters (C and k) and material properties of metals included in Fig. 5

Investigators	C	k	Remarks
Coomb	0.52 1.18	0.68 0.46	Torsion Test Lap Shear Test
Wild	0.16 0.60 0.565	0.30 0.39 0.30	Tensile Joint Test 1/15 CPM Shear Joint Test 5 CPM Shear Joint Test
Shine	0.185	0.53	1 Hz Tensile Test
Kitano	0.1538 0.24	0.415 0.410	0.5 Hz
Enke	0.26	0.52	
Guo/Cutionco	0.34	0.49	
Solomon	1.32	0.52	
Guo/Conrad	3.00	0.70	Tensile Test
Kluizennar	0.39	0.51	Tensile Test
Aldrich	1.30 4.72 10.12	0.637 0.653 0.643	Strain-rate 0.1/sec Strain-rate 4 x 10^{-4}/sec Strain-rate 1 x 10^{-3}/sec

the Coffin-Manson fatigue correlations reported for tin-lead eutectic solder by a wide variety of investigators. Some of this variability is likely due to experimental error (e.g., errors in measuring strain due to fixture flexibility), different definitions of failure (e.g., loss of load versus complete fracture), and different metallurgical conditions of the solder (freshly formed versus age softened versus coarsened with substantial grain growth). In an attempt to remove these possible biases, Fig. 4 contrasts the Coffin-Manson properties reported by a subset of the investigators in Fig. 3, where the subset was selected based on similar experimental approaches and control of solder aging. Note that even with this normalization, a significant variability remains.

Stress Modified Coffin-Manson. In an attempt to explore the wide variability in the Coffin-Manson properties of solder, it is useful to examine the reported properties for a variety of other metals as shown in Fig. 5. Note that the fundamental fatigue behavior of these diverse metals is relatively similar to that of solder. The corresponding Coffin-Manson ductility coefficients and exponents are listed in Table 2 along with the reported ductility and ultimate stresses (Manson and Hirschberg, 1964). It is interesting to note that the Coffin-Manson coefficients in these data appear to vary in a consistent manner with ductility and ultimate stress.

Evidence of this possible coupling between failure rate and stress is even more pronounced in some of the solder literature. Figure 6 by Ahmed and Langdon (1983), and Fig. 7 by Aldrich and Avery (1970) both suggest a strong tie between solder failure and strain rate or stress. Because the fatigue properties of ordinary metals are generally found to be independent of

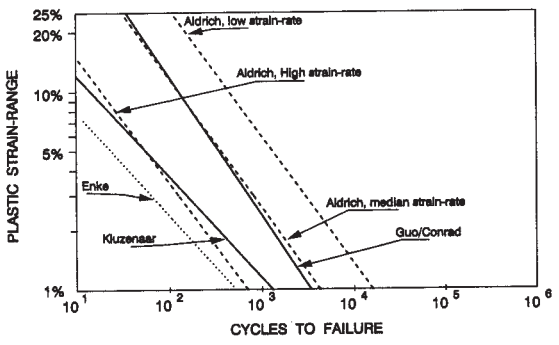

Fig. 4 Coffin-Manson fatigue plots for room-temperature eutectic Sn-Pb solder as reported by a selected subset of investigators

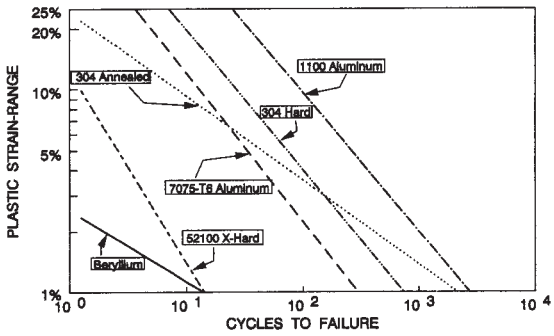

Fig. 5 Coffin-Manson fatigue plots for various metals

frequency, and thus strain rate, the applied stress during loading is suspected as the true determining parameter. Dependency on stress, as opposed to strain rate, is an important distinction, given the strong temperature dependence between strain rate and stress as shown in Fig. 2. If stress is the critical parameter, constant amplitude, constant strain-rate fatigue cycling of solder should result in reduced life at lower temperatures, and vis versa. These data suggest that the Coffin-Manson equation should be augmented with a strain-rate or stress term to account for the strong dependence noted. Using the constitutive properties of solder to convert Aldrich and Avery's data to a stress relationship results in the correlation shown in Fig. 8.

Based on these trends, a modified Coffin-Manson algorithm, which treats the ductility coefficient at a function of maximum solder flow stress σ_m, has been proposed at JPL (Ross and Wen, 1994) and is given by Eq. (2):

$$\Delta\epsilon = C(S/\sigma_m)^{k\gamma}N_f^{-k}$$

or

$$N_f(\sigma_m/S)^{\gamma}\Delta\epsilon^{1/k} = C \tag{2}$$

where

S = reference ultimate stress, 77 ksi
σ_m = maximum flow stress amplitude, ksi
C = ductility coefficient, 0.92
γ = stress exponent, 0.74
k = ductility exponent, 0.7

The constants and exponents of Eq. (2) were determined by best fitting the equation to the experimental results shown in Fig. 4. Note that the results by Enke et al. (1989) and Kluizenaar (1990) were performed with high cycling rates resulting in a high flow stress around 20 ksi, whereas the results obtained by Guo et al. (1990) were performed with a medium strain rate, with a maximum stress level around 5 ksi. The inelastic strain range and maximum flow stress level were computed with the JPL finite element program which makes use of the solder constitutive properties in Figs. 1 and 2.

Table 2 Coffin-Manson parameters (C and k) corresponding to various solder investigators included in Figs. 3 and 4

Metal	C	k	Ductility	Ultimate Stress (ksi)
Beryllium	0.02541	0.353	0.017	46.9
AISI 52100 (Extra Hard)	0.12270	0.944	0.011	362.6
304 Annealed	0.24120	0.415	1.368	108.0
304 Hard	0.97650	0.693	1.165	138.0
7075-T6 Al	0.64920	0.732	0.327	89.9
1100 Al	2.25800	0.685	2.090	16.2

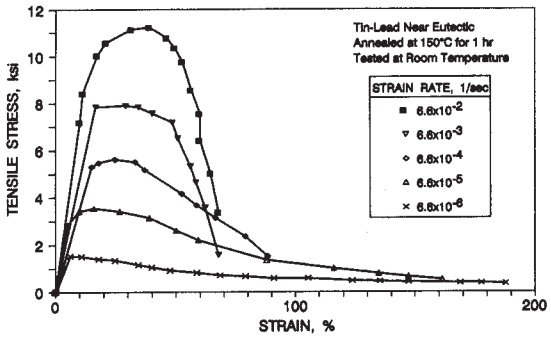

Fig. 6 Strain-rate hardening for near-eutectic solder as reported by Ahmed and Langdon (1983)

The fatigue failure relationship of Eq. (2) is plotted in Fig. 9 and appears as a family of Coffin-Manson curves with maximum stress as a parameter. Each Coffin-Manson curve in Fig. 4 can thus be interpreted as corresponding to a different cyclic peak stress level.

Strain-Energy Based Approach. In contrast to the Coffin-Manson strain-life relationship, a strain energy approach to fatigue assumes the fatigue life is correlated to a cumulative stored visco-plastic strain energy density ΔW with the power-law relationship defined by Eq. (3) (Morrow, 1964):

$$\Delta W(N_f)^{\gamma} = C_e \tag{3}$$

where

$\Delta W = \int \sigma d\epsilon_p$

C_e = material constant

The strain energy density ΔW, when integrated with a stress-strain work hardening relationship, can be expressed as a function of plastic strain range only. In other words, the strain energy approach can be thought of as another variant of the Coffin-Manson equation. The γ exponent is reported by Clech (1993) to be around 0.8, which is somewhat higher than the exponent k in the Coffin-Manson equation.

Analogous to the extension of the basic Coffin-Manson equation to the stress modified C-M correlation, the strain-energy density method can be extended to include both the cyclic strain energy density and inelastic strain range (Sharif et al., 1991) as shown in Eq. (4):

$$\Delta\epsilon_p = C_d(\Delta W)^{-k\gamma}N_f^{-k} \tag{4}$$

where

ΔW = inelastic cyclic strain energy density function, lb-in/in^3

k = ductility exponent, 1.52

γ = work density exponent, 0.77

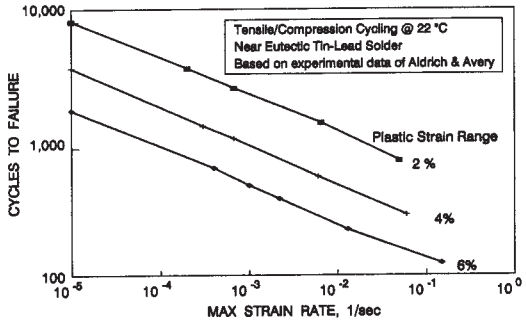

Fig. 7 Solder fatigue life dependence on strain-rate as reported by Aldrich and Avery (1970)

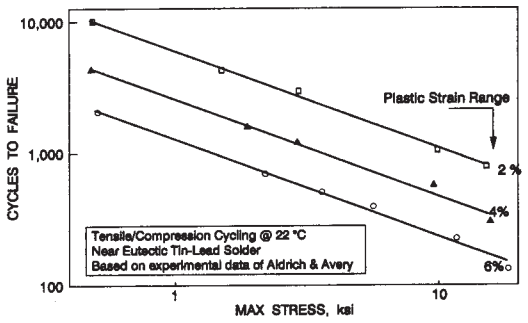

Fig. 8 Solder fatigue life plotted as a function of maximum flow stress

C_d = reference ductility constant, 40000

The constants and exponents of Eq. (4) were determined by best fitting the equation to the experimental results shown in Fig. 4 using a procedure similar to the procedure used to calibrate the stress modified Coffin-Manson equation.

Test Case: Measured Life of Typical LCCs

To provide an experimental evaluation of the various life prediction algorithms discussed above, each was implemented with JPL's finite element stress-strain prediction program, and the analysis predictions were compared with the experimental results of a carefully controlled test program. The test program employed three sets of 50-mil-pitch leadless alumina ceramic chip carriers (Ceramic Quad Flat Packs, CQFP) soldered to single-layer epoxy-fiberglass FR-4 coupons. The three different sizes of LCCs were selected to demonstrate the sensitivity of solder joint service life to part dimensions, and therefore to strain range. The configuration and dimensions of the selected parts of 20, 28, and 68 terminations are presented in Fig. 10. The solder joint fillet profiles of the mass reflowed parts varied somewhat with the part type and castellation geometry, and are shown in Fig. 11.

After soldering, all test articles were placed in a temperature chamber and cycled according to the standard 4-hour NASA cycle from −55°C to +100°C (see Fig. 12).

Two independent damage detection methods were used to quantify the failure statistics: electronic monitoring, and visual inspection. Electronic monitoring detected open-circuit interruptions that lasted longer than 0.25 microseconds. This was done by daisy-chaining the solder joints of each part together, and then connecting the circuit to an Anatech event detector. Visual inspections were also conducted at regular intervals to note the level of observable stressing and cracking.

Figure 13 shows the failure test results in terms of cumulative damage for the 68 pin LCC test articles with a sample size of 20. The first failure was detected by the Anatech device after 53 cycles, while the last (the 20th) sample failed after 139 cycles. The mean life (50 percent probability of failure) is

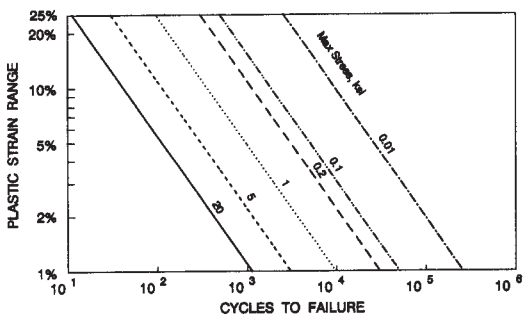

Fig. 9 Stress-modified Coffin-Manson relationship

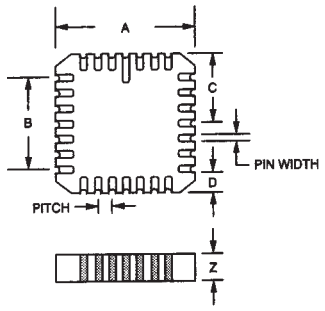

NOMENCLATURE	68 PIN (inches)	28 PIN (inches)	20 PIN (inches)
A	0.950	0.450	0.350
B	0.800	0.300	0.200
C	0.475	0.225	0.175
D	0.0625	0.0625	0.0625
Z	0.083	0.069	0.069
PITCH	0.050	0.050	0.050
PIN WIDTH	0.025	0.025	0.025

Fig. 10 Dimensions of LCC parts use in thermal-cycle test program

around 90 cycles. The test data were fitted with a Weibull distribution curve with a characterization constant C of 97 (i.e., at a failure distribution of 63.2 percent) and a Weibull shape parameter m of 5.

Similar to the cumulative failure distribution shown in Fig. 13, where open-circuiting is used as the definition of failure, additional cumulative damage distributions were developed based on the set of visual degradation criteria. These included heavy stress, crack initiation, partial crack formation, and complete cracking. Figure 14 shows the cumulative damage distributions based on these criteria. Notice that there is an excellent correlation between the cumulative distribution of fully cracked joints in comparison with the data obtained via the Anatech device, i.e., electronically. The mean lives corresponding to crack initiation and fully cracked are 60 cycles and 92 cycles, respectively. This agrees with the contemporary wisdom that when surface crack initiation is detected on LCCs, the major fraction of the solder joint service life has already been consumed.

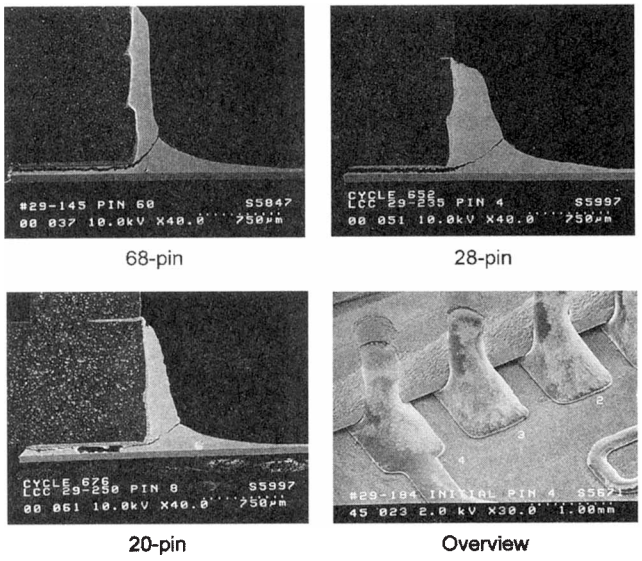

Fig. 11 SEM cross-sections showing different size solder fillets and eventual fracture paths for 68-, 28-, and 20-pin LCCs in JPL thermal-cycle test program

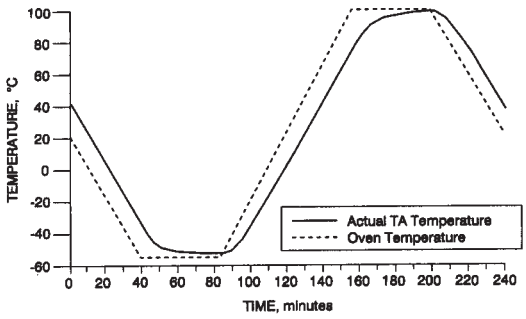

Fig. 12 Temperature profile of 4-hour −55°C to +100°C thermal cycle

In contrast to the 68-pin LCC results, Fig. 15 presents the cumulative failure distributions as determined by electrical open-circuiting for the 28- and 20-pin LCCs. The 20-pin LCCs had a sample size of 8; the first failure occurred at the 573rd cycle and the last 863rd cycle. The 28-pin LCC had a sample size of 31; the first and the last failure were recorded at the 352nd and the 908th cycle, respectively. It is interesting to note that the two failure distribution curves are almost indistinguishable. This is accidental, but predictable, due to the difference in part size exactly off-setting the difference in fillet height. The mean life (50 percent failure probability) is around 660 cycles. The test data were fitted with a Weibull distribution curve with a characterization constant C of 690 (i.e., at a failure distribution of 63.2 percent) and a Weibull shape parameter m of 8. In comparison, the 68-pin LCC test articles had a mean of 90 cycles and a Weibull slope of 5.

Comparison of Predicted Versus Measured Life

The test data obtained with the 68-pin LCCs were used to calibrate each of the failure algorithms discussed above. This was done by adjusting the multiplicative constant C in each equation to force agreement between the model and the measured 68-pin mean life of 90 cycles. Once calibrated, the models were then used to predict the mean fatigue lives for the 28- and 20-pin samples. The analytical results were then compared with the test data as an assessment of the accuracy/utility of each of the models.

Coffin-Manson Algorithm. Using the various individual Coffin-Manson curves in Fig. 3, the predicted cycle life of the 68-pin LCCs range from a low of 3 cycles to a high of 1300 cycles; this is in contrast to the measured life of 90 cycles. To predict the lives of the 20- and 28-pin LCCs, each curve was calibrated by adjusting its "C" value in Eq. (1) so as to accurately predict the measured 90-cycle life. Following calibration, the predictions for the lives of the 28-pin LCCs range from 600

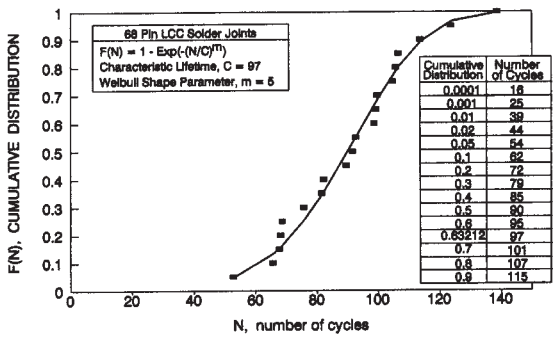

Fig. 13 Cumulative distribution of open-circuit failures for 68-pin LCCs after exposure to 4-hour −55°C to +100°C thermal-cycle test

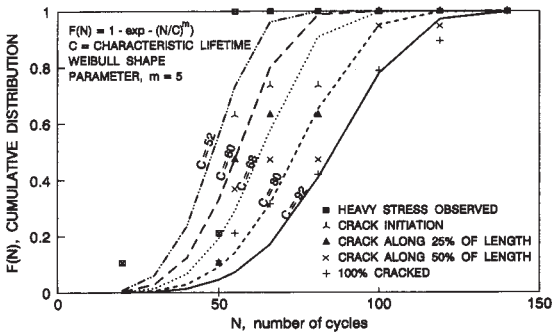

Fig. 14 Cumulative distribution of visual damage for 68-pin LCCs after exposure to 4-hour −55°C to +100°C thermal-cycle test

to 7515 cycles, and for the 28-pin LCCs, range from 562 to 6459 cycles; recall that the measured lives of the 28- and 20-pin LCCs are around 660 cycles. Because the C-values were calibrated, the difference in the Coffin-Manson slopes (k) is responsible for the final variability in the predicted fatigue lives. The long-life predictions (near 7000 cycles) correspond to k values near 0.3, whereas the shorter life predictions (near 600 cycles) correspond to k values near 0.7. An excellent match to the measured lives of the 28- and 20-pin LCCs in this particular temperature-cycle environment is obtained with a k-value of around 0.64.

It should be noted that this particular k-value provides the most accurate predictions in this case, but should not be construed as a universally preferred or "correct" value for other cases. An important case-specific variable is the relative peak stress reached in each solder joint; this can vary significantly from case to case depending on the solder fillet geometry, mean temperature, temperature cycle depth, and cycle rate.

Stress Modified Coffin-Manson Algorithm. In this case, instead of using the simple Coffin-Manson equation, the failure algorithm was replaced by Eq. (2), which includes both strain range and maximum stress during the cycle. Like the above Coffin-Manson cases, this model was first calibrated using the 68-pin test results. With a calibrated C-value of 5.43, the model computes fatigue cycles of 90, 753, and 699 cycles for the 68-, 28- and 20-pin LCCs, respectively. This is in relatively good agreement with the measured test results.

Strain-Energy Based Algorithms. The strain energy density functions for the 68-, 28- and 20-pin LCCs were computed by the JPL finite element program as 195, 31.7, and 33.97 lb-in/in^3, respectively. Using Eq. (3), the uncalibrated life prediction for the 68-pin LCCs was 159 cycles. After adjusting the C-value to achieve the measured 68-pin life of 90 cycles, the life predictions for the 28- and 20-pin LCCs are 872 and 799 cycles, respectively. These also are in modestly good agreement with the measured test results.

Modified Energy Density Algorithm. Similar to the case of the stress modified Coffin-Manson algorithm, the modified energy density equation, Eq. (4), includes both the strain-energy density and the strain range level; the basic energy density function includes only the energy density.

As with the other algorithms, the model was first calibrated to achieve the 90-cycle life prediction for the 68-pin configuration. This provided a calibrated C-value of 40400. The calibrated model was then applied to the 28- and 20-pin stress-strain predictions to obtain life prediction values of 873 and 803 cycles, respectively. These are essentially unchanged from those from the basic strain-energy based algorithm.

Summary and Conclusions

A key part of the solder joint life prediction process is the algorithm used to relate the stresses and strains developed within a solder joint to the level of damage accumulated, and to the probability of ultimate solder joint failure.

Although the basic Coffin-Manson equation provides a serviceable damage accrual algorithm for classes of similar applications, the wide variability in reported Coffin-Manson properties for solder creates large uncertainties whenever new parts or environments are considered. This is particularly true when comparing leaded with leadless parts, and when comparing operation at widely different temperatures. Examination of the solder literature suggests that a possible correlation exists between the Coffin-Manson scatter, and the level of stress generated during the plastic/creep straining process. Solder is fairly unique among metals in that this flow stress is a strong function of strain rate and temperature in most practical applications.

In an attempt to address these observed dependencies, researchers have proposed the use of the strain energy algorithms and the stress-modified Coffin-Manson algorithm discussed here. This paper has examined the life prediction ability of these algorithms together with the basic Coffin-Manson algorithm to predict the thermal-cycle lives of typical 68-, 28-, and 20-pin LCCs. The findings support the use of the stress and strain-energy augmented algorithms, but additional comparisons that involve different mean temperatures and different stress regimes are needed to bolster the observations and provide definitive conclusions. A key issue is the slope-factor k of the Coffin-Manson plot, and the extent to which this factor can be selected with confidence for a particular application.

Although the presented data have focused on the ability of the algorithms to scale between different part sizes, i.e., different strain ranges, additional elements of the overall JPL study have examined the possible influence of the finite element model precision (number of elements) and crack propagation mechanics (Ross et al., 1993, and Ross and Wen, 1994). Thus far, life prediction results have been found to be rather insensitive to the granularity of the finite element model and to the crack propagation dynamics, so long as the failure algorithm is calibrated for the particular model in use. However, the crack propagation model used in conjunction with the stress modified Coffin-Manson equation, Eq. (2), has thus far yielded the most satisfactory analytical results. This modestly improved life-prediction performance is tempered by the very long computer time required for the crack propagation simulation.

In summary, the sensitive drivers controlling the accuracy of fatigue life prediction appear to be the failure prediction algorithm, and the need to capture the time- and temperature-dependent properties of the solder. These drivers are felt to be key to improving our understanding of the creep/fatigue failure of solder, and are particularly important in thermal-cycle applications where the creep strain and flow stress vary considerably.

Acknowledgment

The work described in this paper was carried out by the Jet Propulsion Laboratory, California Institute of Technology,

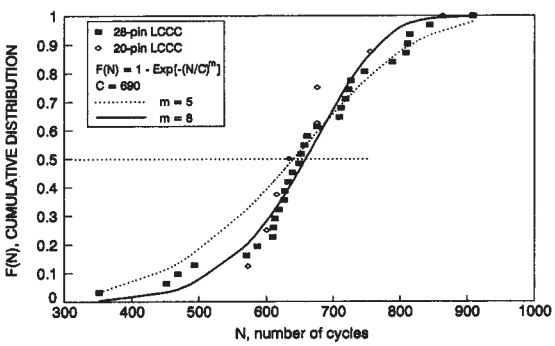

Fig. 15 Cumulative distribution of open-circuit failures for 28- and 20-pin LCCs after exposure to 4-hour −55°C to +100°C thermal-cycle test

under contract with the National Aeronautics and Space Administration. The authors would like to especially thank Ms. Elizabeth Jetter who generated most of the figures used in this paper, Dr. John Winslow and Jack Kovak, who assembled the test boards and conducted the thermal-cycle tests, and Ken Evans, who conducted the Scanning Electron Microcopy.

References

Aldrich, J. W., and Avery, D. H., 1970, "Alternating Strain Behavior of a Superplastic Metal," *Ultrafine Grain Metals,* Proceedings of the 16th Sagamore Army Material Research Conference, Aug. 1969, Syracuse University Press, pp. 397–416.

Ahmed, H. M. I., and Langdon, T. G., 1983, "Ductility of Superplastic Pb-Sn Eutectic at Room Temperature," *J. of Material Science Letter,* No. 2, pp. 59–62.

Avery, D. H., and Backofen, W. A., 1965, "A Structural Basis for Superplasticity," *Trans. ASME,* Vol. 58, pp. 551–562.

Clech, J-P. M., et al., 1993, "A Comprehensive Surface Mount Reliability Model (CSMR) Covering Several Generations of Packaging and Assembly Technology," *Proceedings of 43rd Electronic Components & Technology Conference,* June, pp. 62–70.

Cline, H. E., and Alden, T. H., 1967, "Rate Sensitive Deformation in Tin-Lead Alloy," *Trans. ASME,* Vol. 239, pp. 710–714.

Coffin, L. F., Jr., 1954, "A Study of the Effects of Cyclic Thermal Stresses on a Ductile Metal," *Trans. ASME,* Vol. 76, pp. 931–950.

Coombs, V. D., 1972, "An investigation of Fatigue Life Performance in Lap-type Solder Joints," *Testing for Prediction of Material Performance in Structures and Components,* ASTM STP 515, pp. 3–21.

de Kluizenaar, E. E., 1990, "Reliability of Solder Joint: A Description of the State of the Art—Part I," *Soldering and Surface Mount Technology,* Vol. 4, Feb., pp. 27–38.

Enke, N. F., et al., 1989, "Mechanical Behavior of 60/40 Tin-Lead Solder Lap Joints," *IEEE Trans. CHMT,* Vol. 12, No. 4, Dec., pp. 459–468.

Engelmaier, W., 1989, "Surface Mount Solder Joint Long-term Reliability: Design, Testing, Prediction," *Soldering and Surface Mount Technology,* Vol. 1, Feb., pp. 12–22.

Guo, Z., et al., 1990, "Effect of Composition on the Low-Cycle Fatigue of Pb Alloy Solder Joints," *Proceedings of the 40th Electronic Components and Technology Conference,* May 20–23, Las Vegas, NV, pp. 496–506.

Guo, Q., et al., 1992, "Thermomechanical Fatigue Life Prediction of 63Sn/37Pb Solder," ASME JOURNAL OF ELECTRONIC PACKAGING, Vol. 114, No. 2, June, pp. 145–150.

Kitano, M., Kawai, S., and Shimizu, I., 1988, "Thermal Fatigue Strength Estimation of Solder Joints of Surface Mount IC Packages," *Proceeding 8th Annual Int. Elect. Packaging Conf.,* IEPS, Dallas, Texas, Nov., pp. 4–11.

Manson, S. S., 1953, "Behavior of Materials under Conditions of Thermal Stress," *Heat Transfer Symposium,* Univ. of Michigan Engineering Research Institute, pp. 9–95.

Manson, S. S., and Hirschberg, M. H., 1964, "Fatigue Behavior in Strain Cycling in the Low- and Intermediate-Cycle Range," *Fatigue—An Interdisciplinary Approach,* Proceedings of the 10th Sagamore Army Material Research Conference, Syracuse University Press, pp. 133–185.

Morrow, J. D., 1964, "Cyclic Plastic Strain Energy and Fatigue of Metals," ASTM STP 378, ASTM, pp. 45–87.

Murty, G. S., 1973, "Stress Relaxation in Superplastic Materials," *J. of Material Science,* Vol. 8, pp. 611–614.

Ross, R. G., Jr., et al., 1992, "Creep-Fatigue Interactions with Flexible Leaded Parts," ASME JOURNAL OF ELECTRONIC PACKAGING, Vol. 114, No. 2, June, pp. 185–192.

Ross, R. G., Jr., and Wen, L., 1993, "Solder Joint Creep and Stress Relaxation Dependence on Construction and Environmental-Stress Parameters," ASME JOURNAL OF ELECTRONIC PACKAGING, Vol. 115, June, pp. 165–172.

Ross, R. G., Jr., and Wen, L., 1994, "Crack Propagation in Solder Joints During Thermal-Mechanical Cycling," ASME JOURNAL OF ELECTRONIC PACKAGING, Vol. 116, No. 2, June, pp. 69–75.

Sharif, I., Barker, D., Dasgupta, A., and Pecht, M., 1991, "Fatigue Analysis of a Planarpak Surface Mount Component," ASME JOURNAL OF ELECTRONIC PACKAGING, Vol. 113, June, pp. 194–199.

Shine, M. C., and Fox, L. R., 1988, "Fatigue of Solder Joint in Surface Mount Devices," *Low Cycle Fatigue,* STM STP 942, H. D. Solomon, et al., eds., ASTM, pp. 588–610.

Solomon, H. D., 1985, "Low Cycle Fatigue of 60/40 Solder—Plastic Strain Limited vs. Displacement Limited Testing," *Proceedings of ASM's 2nd Electronic Packaging: Materials and Processes Conference,* Bloomington, MN, Oct., pp. 29–47.

Weinbel, R. C., Tien, J. K., Pollak, R. A., and Kang, S. K., 1987, "Creep-Fatigue Interaction in Eutectic Lead-tin Solder Alloy," *J. of Material Science Letter,* Vol. 6, pp. 3091–3096.

Wild, R. N., 1975, "Some Fatigue Properties of Solders and Solder Joints," IBM Report, No. 74Z00481, IBM Federal Systems Division, New York.

Zehr, S. W., and Backofen, W. A., 1968, "Superplasticity in Lead-Tin Alloys," *Trans. ASME,* Vol. 61, pp. 300–312.